Electronic Supplementary Material (ESI) for Journal of Materials Chemistry A.

Enhancing the kinetics of lithium–sulfur battery under solid−state conversion by using tellurium as a eutectic accelerator

Shuping Li[a], Jingqi Ma[a, b], Ziqi Zeng[a], Wei Hu[a], Wei Zhang[a], Shijie Cheng [a, *], Jia Xie[a, *]

[a] State Key Laboratory of Advanced Electromagnetic Engineering and Technology, School of Electrical and Electronic Engineering Huazhong University of Science and Technology Wuhan 430074, P. R. China
[b] State Key Laboratory of Materials Processing and Die & Mould Technology, School of Materials Science and Engineering, Huazhong University of Science and Technology, Wuhan 430074, P. R. China

E–mail: xiejia@hust.edu.cn

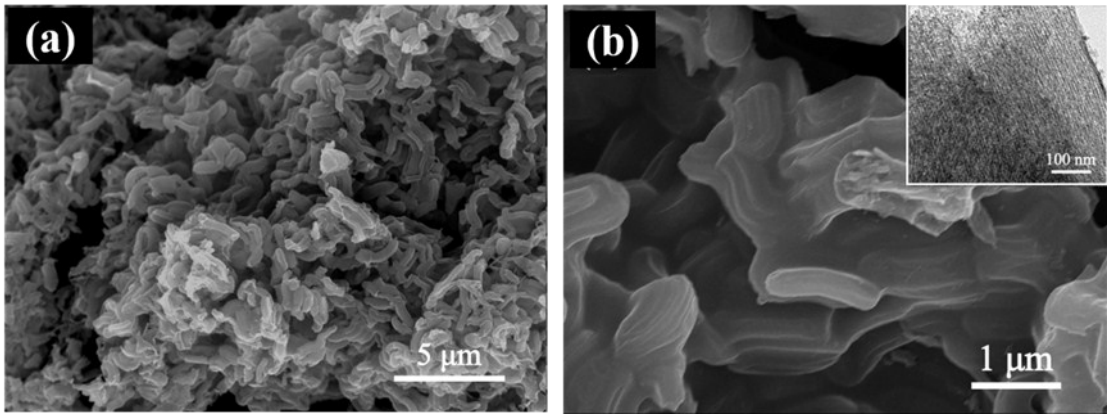

Fig. S1 The scanning electron microscope (SEM) pictures of CMK–3. (a) low magnification; (b) high magnification (the insert is local transmission electron microscope (TEM) picture of CMK–3).

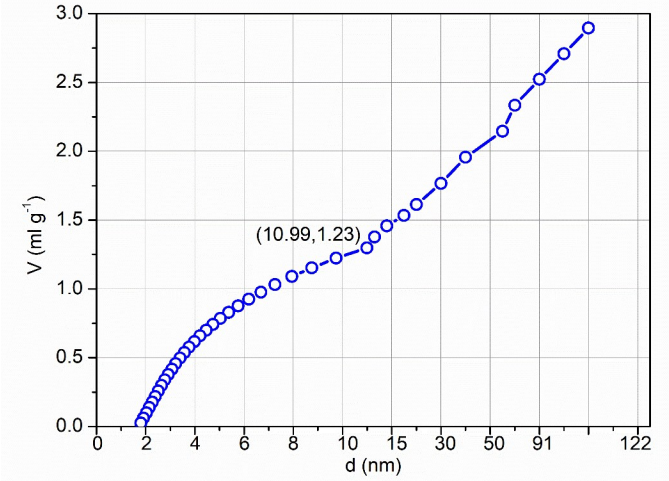

Fig. S2 The relationship between diameter and pore volume.

Based on the BJH adsorption curve, the relationship of the pore volume and pore diameter for CMK–3 is displayed in Fig. S2.

The mesoporous characteristics of CMK–3, and the pore size is about 3–4 nm. Accordingly, in order to encapsulate the sulfur into mesoporous, we only calculate the pore volume under the pore size of less than 10.99 nm (with the pore volume of 1.23 ml g^{-1}). As there is 80% volume expansion from sulfur converting into lithium sulfide, the mass of sulfur is calculated by the equation $m_{sulfur}=D_{sulfur} \times V_{pore} \times 1/(1+80\%)$. As the density of sulfur is 2.36 g ml^{-1}, the mass of sulfur is 1.69 g, and the maximum sulfur content should be 62.8%.

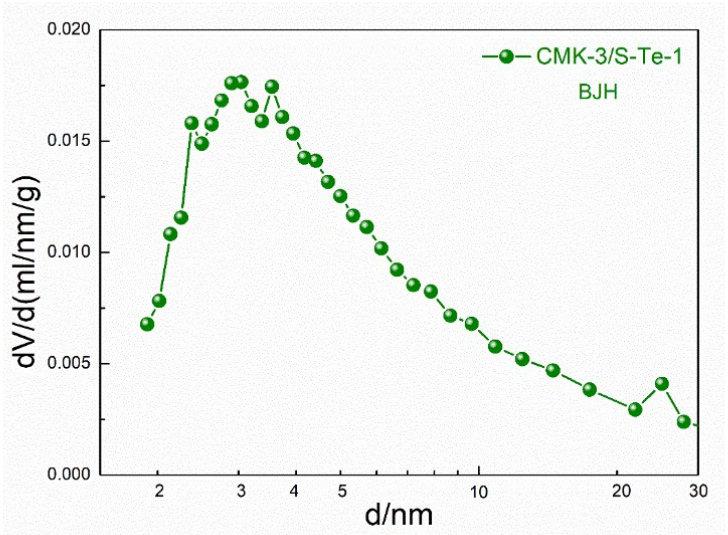

Fig. S3 The BJH distribution of CMK–3/S–Te–1.

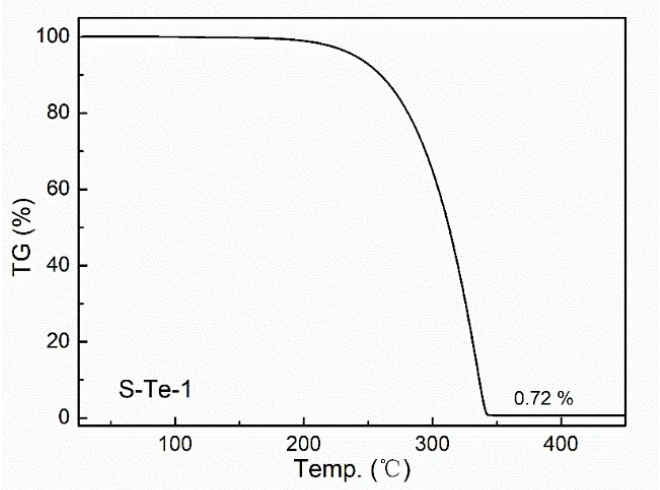

Fig. S4 The thermal gravimetric (TG) curve of S–Te–1.

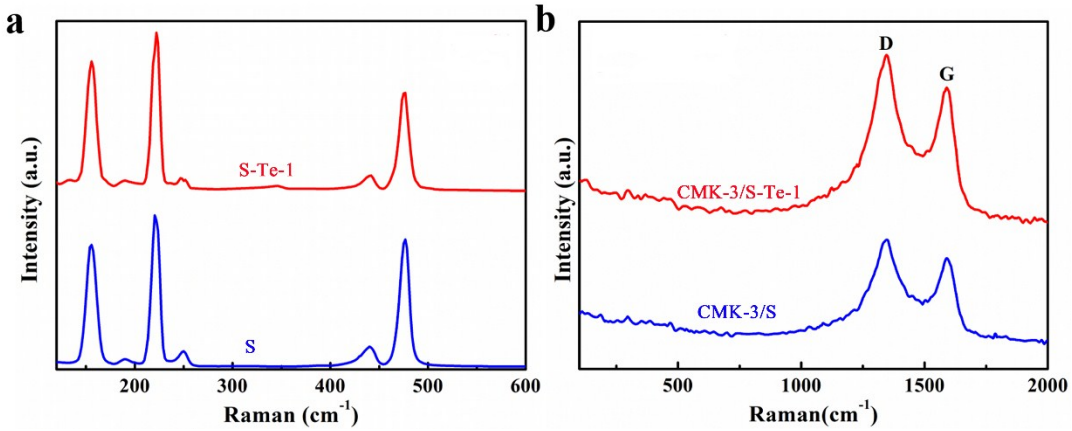

Fig. S5 The Raman spectrum of S and S–Te–1 (a), CMK–3/S and CMK–3/S–Te–1 (b).

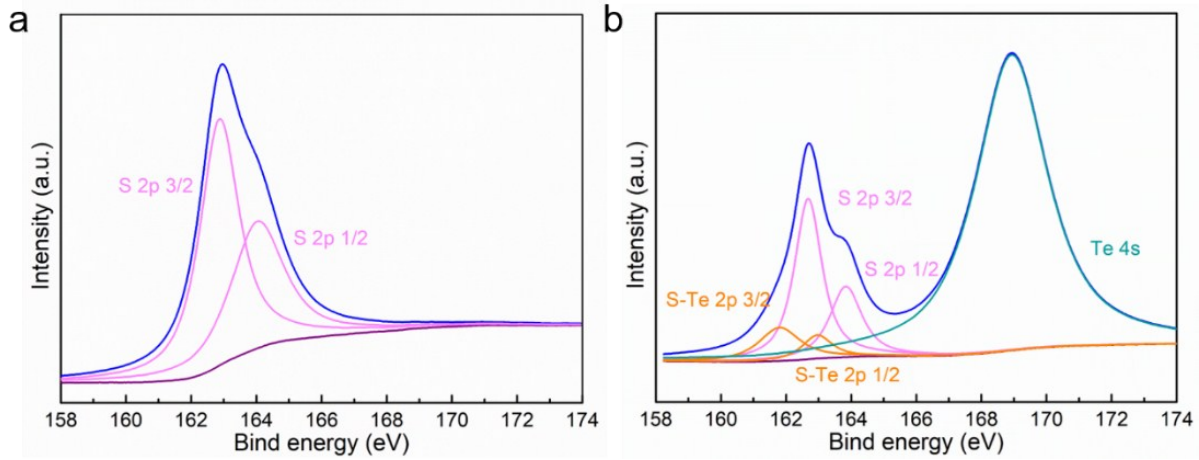

Fig. S6 (a) The high–resolution S 2*p* XPS of pure S. (b) The high–resolution S 2*p* XPS of S–Te–1.

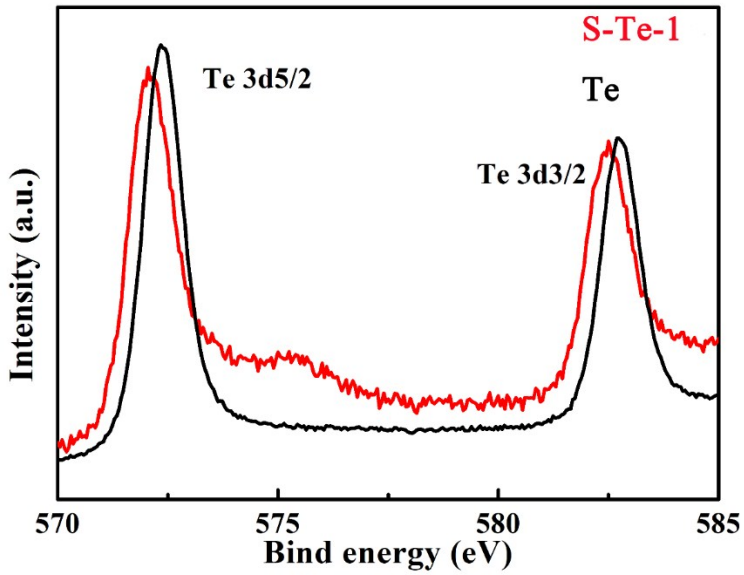

Fig. S7 The high–resolution Te 3*d* X–ray photoelectron spectroscopy (XPS) for S–Te–1 and Te powder.

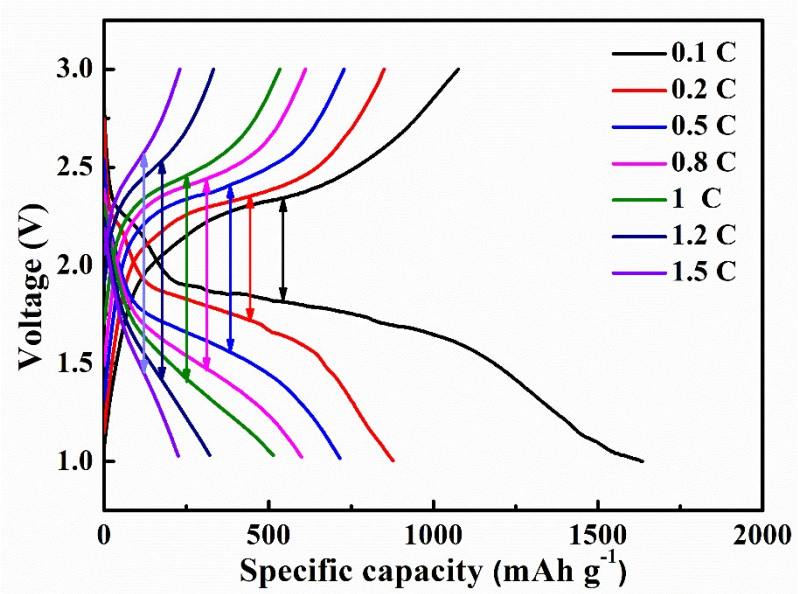

Fig. S8 The voltage–capacity curves of CMK–3/S at various current densities.

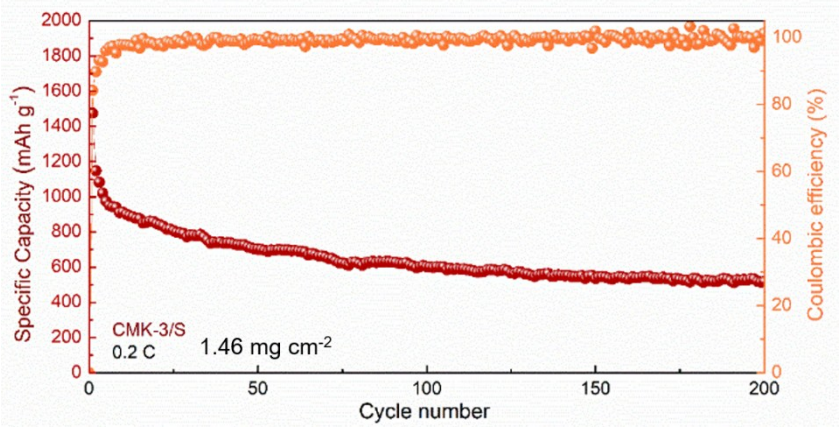

Fig. S9 The long cycle performance of CMK–3/S at 0.2 C.

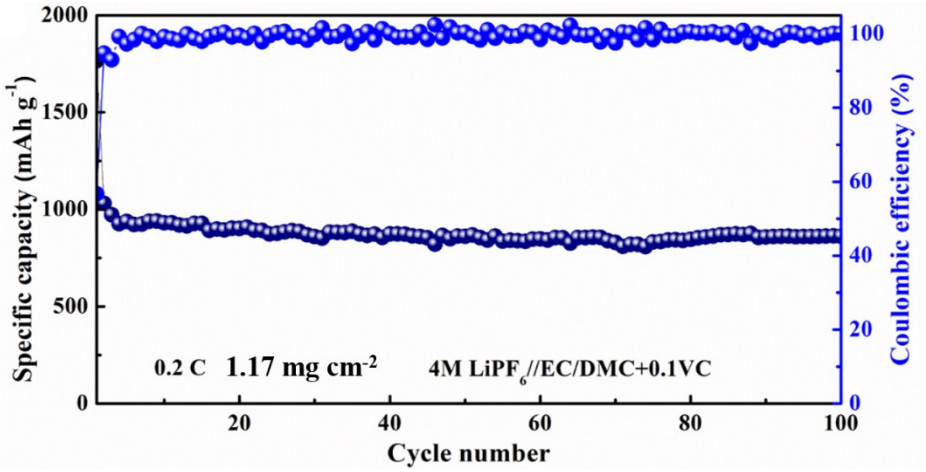

Fig. S10 The long cycle performance of CMK–3/S–Te–1 in the carbonate electrolyte.

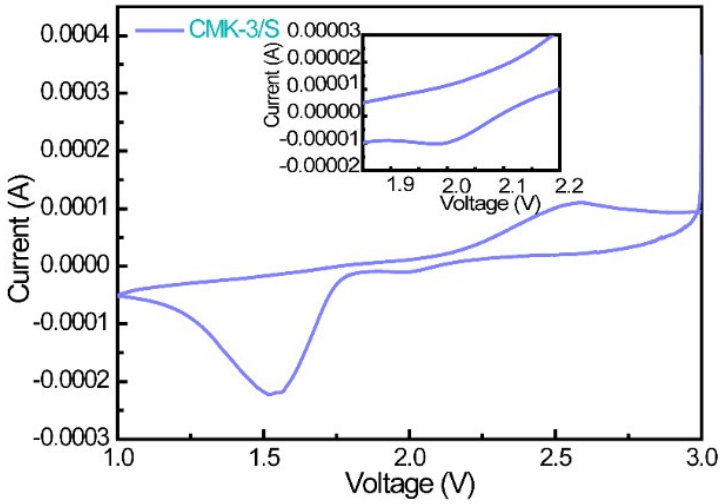

Fig. S11 The initial CV curve of CMK–3/S cathode (the insert is the enlarged picture of the first reduction peak).

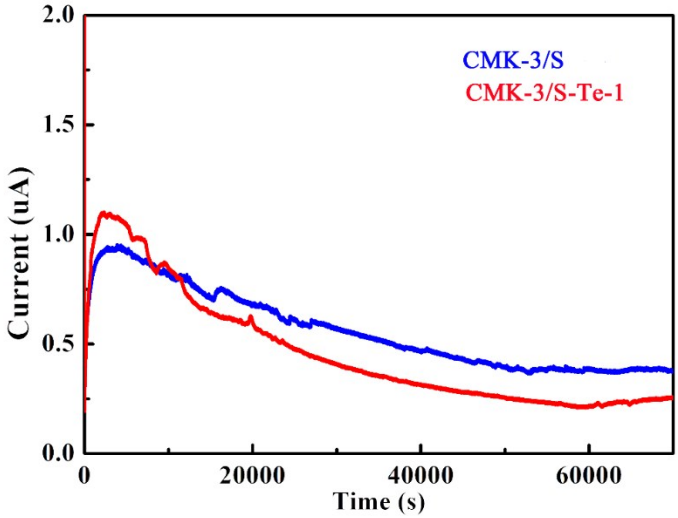

Fig. S12 The shuttle current test of CMK–3/S–Te–1 and CMK–3/S cathodes in the ether electrolyte.

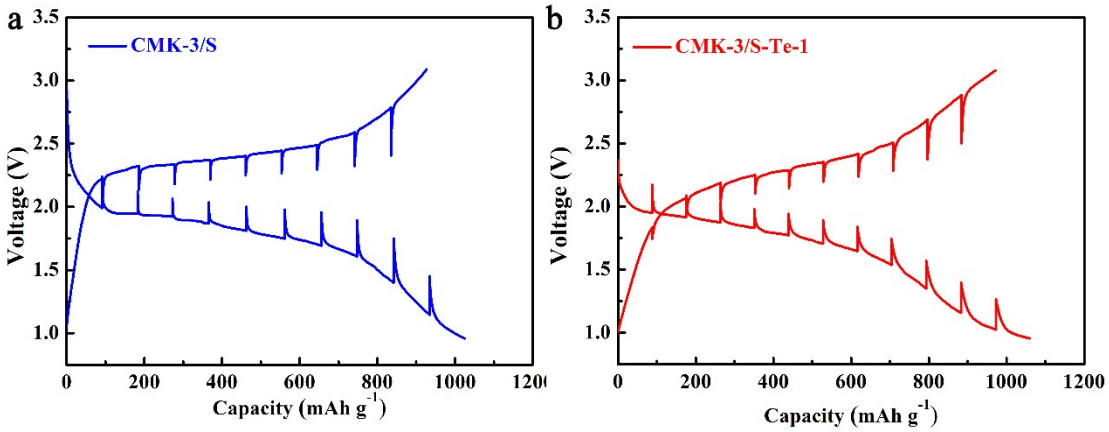

Fig. S13 The GITT curves of CMK–3/S (a) and CMK–3/S–Te–1 (b) at 1/30 C.

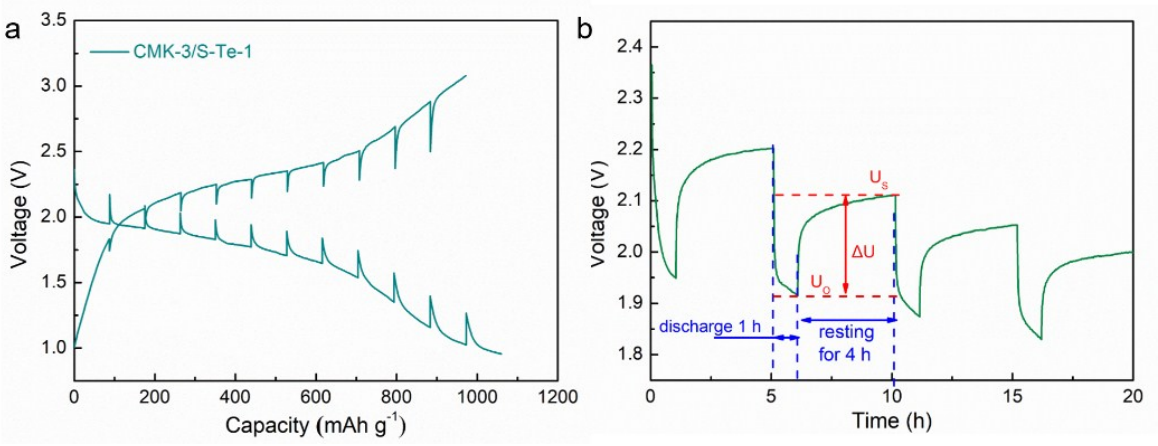

Fig. S14 (a) The GITT curves of CMK–3/S–Te‑1, (b) The time–voltage curve of CMK–3/S–Te‑1 cathode at initial hours.

The reaction resistance R is calculated by the equation $R = \frac{\Delta U}{Im_s}$

Where, $\Delta U = U_S - U_O$, U_O is the original voltage after discharge for 1h, and U_S is the stable voltage after resting for 4 h. m_s is the active material mass of sulfur. I is the discharge current which equals to discharge current density 1/30 C (55.8 mA g^{-1}) multiply by m_s. (ACS Energy Lett. 2018, 3, 420–427)

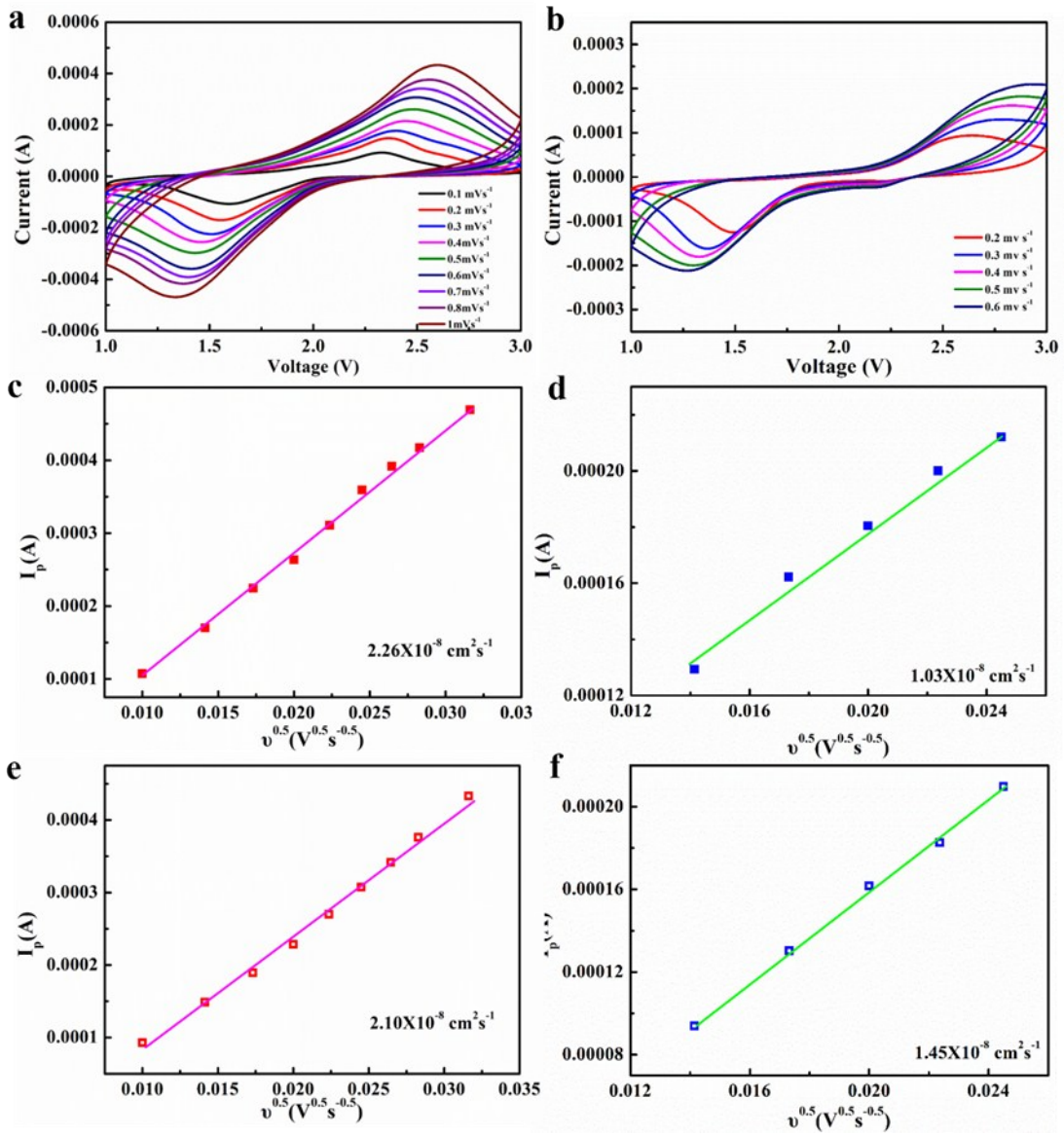

Fig. S15 CV curves at various scan rates for CMK–3/S–Te–1 (a) and CMK–3/S (b). The line fitting of peak currents versus square root of scan rates for CMK–3/S–Te–1 (c) reduction and (e) oxidation peaks in an ether electrolyte, respectively. The line fitting of peak currents versus square root of scan rates for CMK–3/S for (d) the reduction and (f) oxidation peaks in an ether electrolyte, respectively.

Lithium–ion diffusion coefficients for CMK–3/S and CMK–S–Te–1 cathodes were calculated by a series of cyclic voltammograms curves with various scan rates and were analyzed with Randles–Sevick equation. $Ip= 2.69 \times 10^5 n^{1.5} AD_{Li}{}^{+\,0.5} C_{Li}{}^{+} v^{0.5}$

In the equation, I_p represented the peak current (A), n was the number of electrons transformation in the reaction (2 for lithium sulfur battery), $C_{Li}{}^{+}$ represented the lithium ion concentration (mol L^{-1}) and v referred to the scanning rate (V s^{-1}). A was the area of electrode (cm^2), which was unknown due to the porosity of the electrode. $D_{Li}{}^{+}$ stood for lithium–ion diffusion coefficient (cm^2 s^{-1}), Hence, $AD_{Li}{}^{+}$ was calculated and $AD_{Li}{}^{+}$ ratio of CMK–3/S and CMK–3/S–Te–1 was used to value the capability of lithium–ion diffusion coefficient.

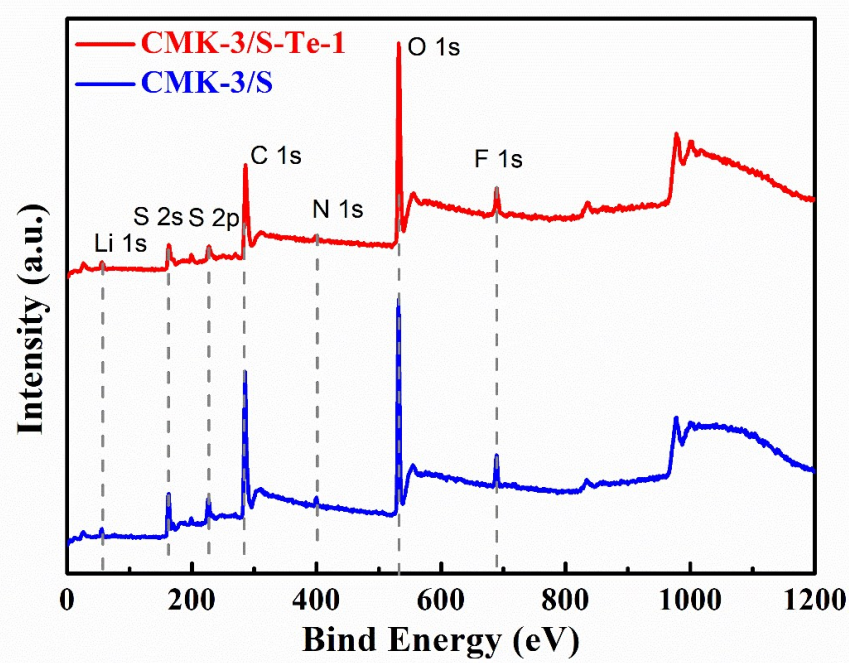

Fig. S16 The wide XPS spectrum of SEI films on CMK–3/S–Te–1 and CMK–3/S cathodes.

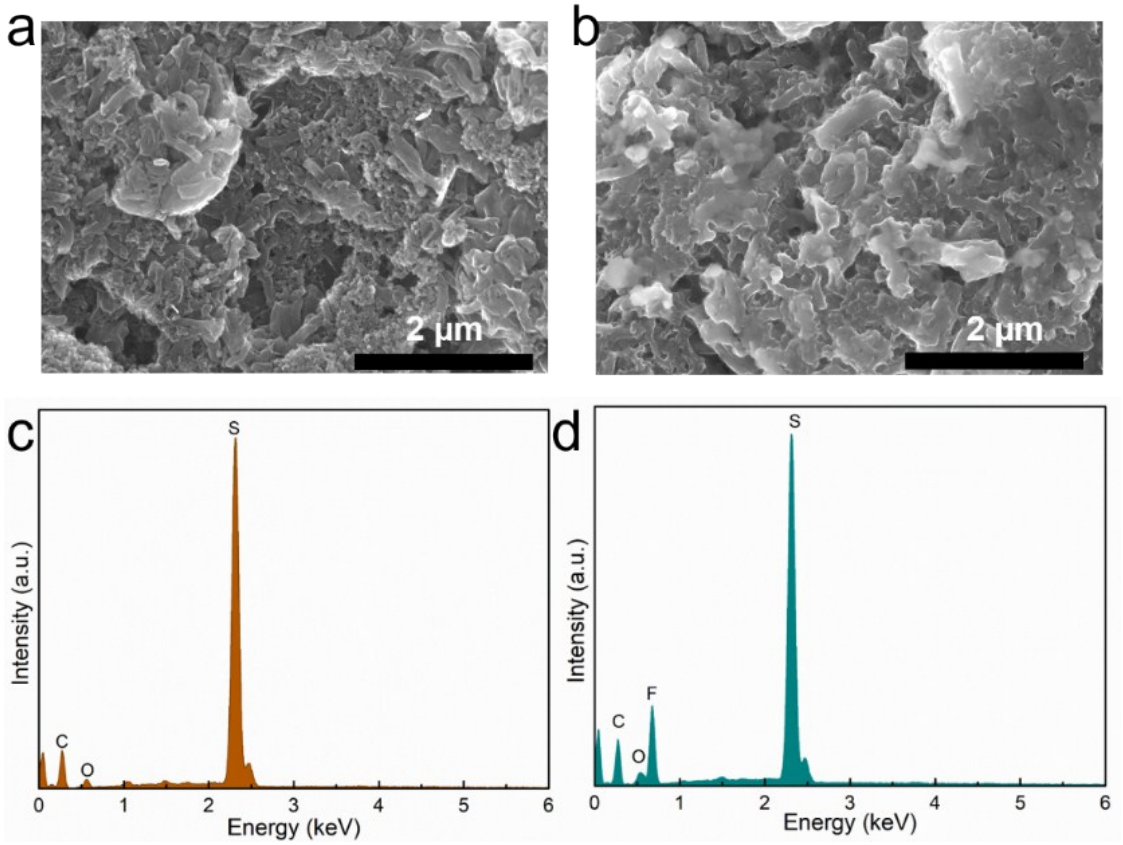

Fig. S17 (a) and (c) The top view SEM picture and EDS of the pristine CMK–3/S electrode. (b) and (d) The top view SEM picture and EDS of CMK–3/S electrode after several cycles.

Table S1. The C 1*s* composition ratios of SEI films on CMK–3/S–Te–1 and CMK–3/S cathodes.

	C–C	C–O	ROCOOLi	Li_2CO_3	–OCOO
CMK-3/S	52.02	32.45	8.29	4.43	2.81
CMK-3/S–Te–1	41.21	31.47	12.80	8.47	6.05

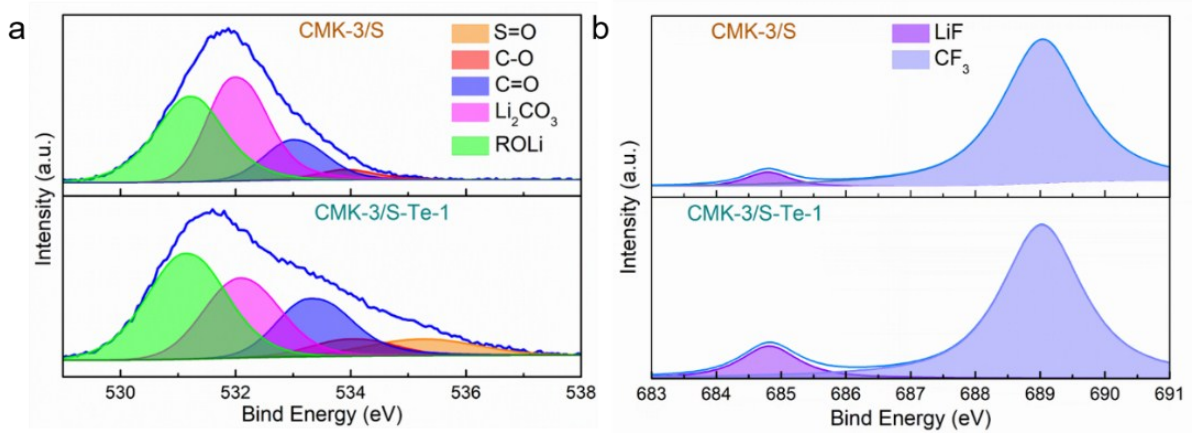

Fig. S18 (a) The high–resolution O 1*s* XPS analysis of the SEI films for both cathodes. (b) The high–resolution F 1*s* XPS analysis of the SEI films for both cathodes.

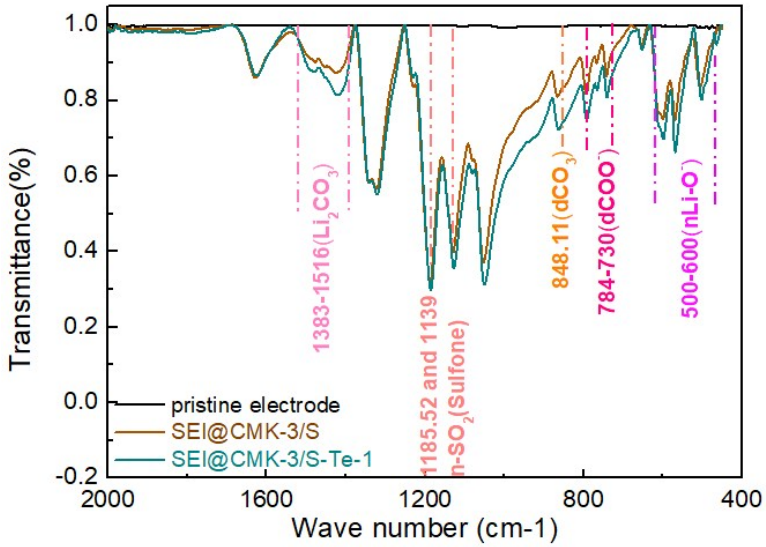

Fig. S19 ATR–FTIR of pristine cathode, SEI@CMK–3/S cathode and SEI@CMK–3/S–Te–1 cathode.

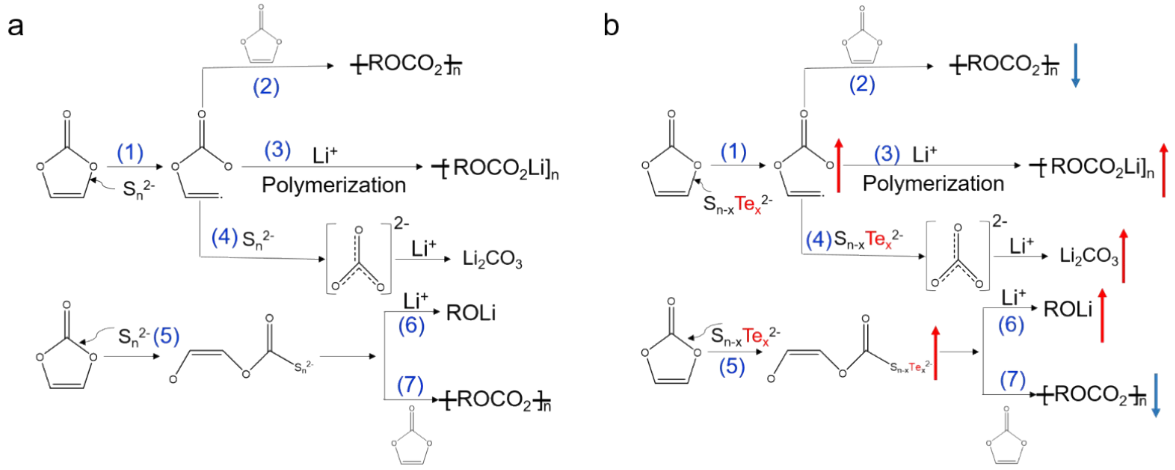

Fig. S20 (a)The proposed nucleophilic reaction on the surface of CMK–3/S (J. Mater. Chem. A, 2018, 6, 23396). (b) The proposed nucleophilic reaction on the surface of CMK–3/S–Te–1 (the blue arrows represent weakened reaction, the red arrows represent enhanced reaction).

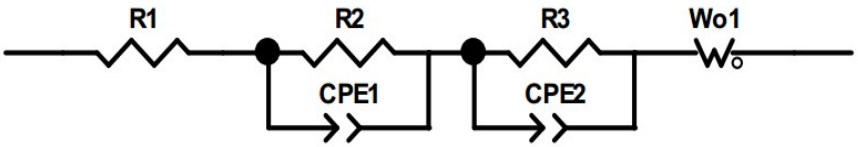

Fig. S21 The schematic of impedance fitting circuit for EIS.

Table S2. The details of the fitting results for EIS.

	CMK–3/S–Te–1	CMK–3/S
R1 (ohm)	20.5	50
R2 (R_{SEI}) (ohm)	47.02	125.1
R3 (R_{CT}) (ohm)	98.5	1337
CPE–1	1.8023E–5	9.7634E–6
CPE–2	6.1287E–4	2.7533E–4

The calculation of relaxation Time:
Characteristic Frequency: f_b**=1/2πRC,** ωRC**=1**
Relaxation Time: τ**=1/ω=RC=1/2π**f_b

Table S3 The Characteristic Frequency and Relaxation Time of R_{SEI} and R_{CT} for CMK–3/S–Te–1 and CMK–3/S.

	CMK–3/S	**CMK–3/S–Te–1**
Characteristic Frequency of $\mathbf{R_{SEI}}$ (Hz)	1001	1470

Relaxation Time of $\mathbf{R_{SEI}}$ (s)	1.59×10^{-4}	1.08×10^{-4}
Characteristic Frequency of $\mathbf{R_{CT}}$ (Hz)	1.212	4.642
Relaxation Time of $\mathbf{R_{CT}}$ (s)	0.13	0.03

Table S4 The estimated areas of SEI films on these surfaces of CMK–3/S and CMK–3/S–Te–1 cathodes.

	CMK–3/S–Te–1	CMK–3/S
BET area (m^2 g^{-1})	54.5	52.3
The mass of powder (mg)	1	1
The area of powder (m^2)	0.0545	0.0523

Table S5. The estimated conductivity values of these SEI films on CMK–3/S and CMK–3/S–Te–1 cathodes.

	CMK–3/S–Te–1	CMK–3/S
Thickness of SEI film (nm)	10	10
R_{SEI} (ohm)	47.02	125.1
Area of SEI film (m^2)	0.0545	0.0523
σ(S m^{-1})	3.9×10^{-9}	1.5×10^{-9}

In order to estimate conductivity values of these SEI films on CMK–3/S and CMK–3/S–Te–1 cathodes, we have made some simplification and hypothesis. At first, we suppose the σ of SEI film can be calculated by the following equation.

$\sigma_{SEI}=L_{SEI}/(R_{SEI}\times S_{SEI})$ (**Nat. Chem. 2019, 11, 789**)

where, L_{SEI} is the thickness of SEI film, which is estimated to be 10 nm, referencing to some articles **(J. Mater. Chem. A, 2018, 6, 23396; Chem. Rev. 2017, 117, 10403**). R_{SEI} is the resistance of SEI film, which can be obtained by fitting analysis the EIS curve. The R_{SEI} values of CMK–3/S and CMK–3/S–Te–1 cathodes are 47.02 and 125.1 ohm, respectively. S_{SEI} is the area of SEI film. Due to the nucleophilic reaction, the SEI films are formed on surfaces of the CMK–3/S and CMK–3/S–Te–1 powders; hence, these areas of SEI films are approximate to these areas of CMK–3/S and CMK–3/S–Te–1 powders. We have known the specific areas and the mass of these powders in each electrode, so these areas of SEI films are known.